Journal of Low Temperature Physics, Vol. 61, Nos. 5/6, 1985

The Temperature and Pressure Dependence of the Normal Fraction of Superfluid ^{3}He-B

J. M. Parpia

Department of Physics, Texas A&M University, College Station, Texas

D. G. Wildes,* J. Saunders,† E. K. Zeise,‡ J. D. Reppy, and R. C. Richardson

Laboratory of Atomic and Solid State Physics, Cornell University, Ithaca, New York

(Received May 24, 1985)

Measurements have been made of the normal fluid fraction of superfluid ^{3}He-B at eight different pressures between 0 and 29.2 bar. The minimum temperatures were such that ρ_n/ρ was reduced to less than 0.5%. The experiments, carried out independently at Cornell and Texas A&M Universities, used similar Andronikashvilli-type torsional oscillators. The results are qualitatively similar, but show significant differences due to the use of different temperature standards. Both sets of results are presented in tabular form. The inconsistencies in the temperature scales preclude the examination of the results for possible strong coupling effects.

1. INTRODUCTION. THE NORMAL FRACTION OF SUPERFLUID ^{3}He-B

The superfluid fraction (superfluid density) of liquid ^{3}He was first measured using fourth-sound resonator techniques,[1,2] strengthening the identification of the extraordinary phases of liquid ^{3}He as being "superfluid." Later measurements of the superfluid density using vibrating wire techniques[3] and parallel plate geometries[4] exhibited temperature dependences which differed from those of the earlier experiments in porous media.[1,2] The anisotropy of the A-phase superfluid density tensor was first observed

*Present address: General Electric Research and Development Center, Schenectady, New York.
†Present address: University of Sussex, Brighton, England.
‡Present address: Eastman Kodak Research Labs, Rochester, New York.

0022-2291/85/1200-0337$04.50/0

using a torsional oscillator device[5] patterned on the classic Andronikashvilli pendulum.[6] Experiments by Archie *et al.*[7] extended these data to normal fluid fractions $\rho_n/\rho \approx 0.2$ and demonstrated that the torsional oscillator technique offers, in principle, a simple method for measuring the temperature and pressure dependence of the order parameter of the superfluid B phase of ^{3}He. The high precision available from the oscillator measurements should allow a determination of the strong coupling corrections to the order parameter. Normal density results are also necessary for determining the dynamic viscosity η from a variety of experiments[8,9] which measure the kinematic viscosity η/ρ_n.

Torsional oscillator measurements of the normal fluid fraction can provide a valuable intermediate standard for the comparison or calibration of thermometers at temperatures between 0.3 and 2.7 mK. The measurements are highly reproducible and provide a particularly sharp indication of the superfluid transition. The oscillators are simple to construct and operate. Finite-size effects[10] have only a small effect on the normal density results, although they can dominate measurements of the viscosity at low temperatures.

The precision of these oscillator experiments does not, however, yield correspondingly precise information on the properties of ^{3}He. This shortcoming is due to the current state of disarray of thermometry in the millikelvin region. These discrepancies have been noted in the literature[11] and have had a significant impact on measurements of the Fermi liquid parameters (in particular F_1^s, derived from specific heat data [8,12]) as well as on attempts to determine the magnitude of the strong coupling corrections.

This paper presents the results of two independent series of measurements of the normal density as a function of temperature and pressure. The data extend to normal fractions $\rho_n/\rho < 5 \times 10^{-3}$, allowing good determination of the "empty cell" period and dissipation of the oscillators. The two experiments have been difficult to relate to each other, due principally to differences in the temperature scales. The Texas A&M scale is based on a lanthanum-diluted cerium magnesium nitrate (LCMN) susceptibility thermometer, calibrated from measurements of the melting curve of ^{3}He. The Cornell thermometry is also based on LCMN susceptibility, but is calibrated from NMR susceptibility measurements on platinum powder. The separate results of the two experiments and a set of smooth interpolating functions for each are presented in tabular form. We wish to draw attention to the significant consequences of the subtle differences in these temperature scales and to emphasize the operational difficulties associated with the extrapolation of LCMN thermometers into the submillikelvin region.

2. CRYOSTATS AND THERMOMETRY

2.1. The Cryostats

The Cornell cryostat[7,8] uses a copper demagnetization stage to cool $\sim 14\,\text{cm}^3$ of liquid ^{3}He to minimum temperatures of ~ 0.35 mK (at 0 bar liquid pressure). The coolant bundle comprises 14 moles of 0.30-mm-diameter copper wire and is precooled to 18.5 mK in a 7.7-T field by a rebuilt SHE model DRP-36 dilution refrigerator. The cryostat warms from $T \approx 0.25\ T_c$ to T_c in ~ 100 h. The pressure in the liquid ^{3}He cells is sensed by a capacitive strain gauge located in a liquid nitrogen dewar outside the cryostat. A simple integrator circuit and a heater in an insulated cell at room temperature serve to regulate the liquid pressure to within ~ 1 mbar.

The Texas A&M cryostat[13] uses a combined $PrNi_5$ and copper demagnetization system to attain minimum temperatures of ~ 0.35 mK and remain below 1.1 mK for periods exceeding 2 weeks. The coolant bundle includes 0.27 mole $PrNi_5$ and 2.8 moles Cu, precooled to 8 mK in 7.8 T by an SHE model 420 dilution refrigerator. The liquid pressure was regulated to within 10 mbar during these runs.

Both research groups observe that the minimum measured temperature is strongly dependent on the pressure in the liquid ^{3}He cell. Relative to the superfluid transition temperature, however, these minima are essentially pressure independent ($T_{\text{min}}/T_c \approx 0.21$ and 0.245 at Cornell and Texas A&M, respectively).

2.2. The Cornell Temperature Scale

The most sensitive thermometer on the Cornell cryostat was a 70-mg pill of lanthanum-diluted cerium magnesium nitrate (LCMN). Polycrystalline LCMN, grown from a solution of 5% CMN and 95% LMN, was powdered and packed to 50% packing fraction. The LCMN susceptibility was monitored by a conventional ac bridge[8] which used an SHE rf SQUID magnetometer, operating in a flux-locked loop, as a null detector. An Intel SBC-80/10 microcomputer monitored the bridge off-balance signal and automatically adjusted a programmable ratio transformer which controlled the in-phase portion of the nulling signal. The remaining error signal was recorded by the computer for subsequent analysis.

The LCMN pill and the bridge excitation and detection coils were housed in a two-part niobium-titanium can to provide isolation from the fringing fields of the main demagnetization coil and the heat switch magnet. The can was perforated at both ends and slots were milled along the sides of the mating halves to provide maximum thermal contact between the

LCMN, the liquid ^{3}He, and the torsional oscillator. All wiring from the LCMN cell to the rf SQUID was run through niobium or solder-plated copper-nickel tubes. A large mu-metal shield was raised around the dewar during each initial cooldown to 4.2 K, to minimize the field trapped in these and other superconducting shields.

The LCMN thermometer provides extraordinary sensitivity ($<0.1\ \mu$K at 1 mK) and may be continuously measured to the lowest temperatures. However, the SQUID magnetometer is not isotope-specific, but senses the total susceptibility of the LCMN and cell; the susceptibility and temperature dependence of the background may become comparable to that of the LCMN at temperatures above a few mK. Additionally, the LCMN is believed to order magnetically at a temperature of $\sim$0.1 mK. These complications, at high and low temperatures, imply that any claim of Curie-Weiss-like behavior for the susceptibility measured by an LCMN thermometer must be verified by comparison to some other, more reliable temperature scale.

The Cornell LCMN was calibrated against a platinum NMR thermometer.[7] The platinum powder was obtained from the Helsinki low-temperature physics group and had previously been calibrated against a nuclear orientation primary thermometer.[14] A cylindrical niobium shield surrounded the NMR coil and was used to trap a static field of 27 mT. Automatic control of the pulsed NMR measurements was provided by a standard controller (model PLM-3, Instruments for Technology, Helsinki, Finland). The parallel BCD outputs of the controller were connected to the microcomputer data acquisition system and recorded for subsequent analysis.

The platinum susceptibility is believed to follow the Curie law with negligible corrections to $T \lesssim 0.1$ mK. In principle, the Curie constant may be calibrated at a single reference temperature (e.g., T_A on the ^{3}He melting curve). Measurements of the susceptibility then define the platinum temperature scale.

The platinum susceptibility is not, however, a good principal thermometer at low temperatures. The spin-lattice relaxation time becomes extremely long, limiting the repetition rate of the NMR pulses. The resolution of the PLM controller is limited to $\sim$0.1%. For these reasons, the platinum is used as a calibration standard for the LCMN, rather than as a direct source of temperature data.

In practice, the Cornell group obtained the platinum Curie constant C_{Pt} by calibration against temperatures determined from the spin-lattice relaxation time T_1 and the Korringa law, $T_1 T = 29.9$ msec K for this powder.[14] The susceptibility and the spin relaxation time were compared over the temperature range $2 \lesssim T \lesssim 30$ mK. Temperatures obtained from the Curie

law behavior of the platinum susceptibility were then used to calibrate the LCMN thermometer.

A Curie-Weiss law was assumed for the LCMN's susceptibility,

$$\chi - \chi_0 = C/(T - \Delta) \tag{1}$$

The limiting high-temperature susceptibility χ_0 was determined by fitting the LCMN susceptibility against the platinum spin-lattice relaxation time T_1 over a temperature range of 15-30 mK. The values of C and Δ were then obtained by fitting the reciprocal of Eq. (1) against the platinum susceptibility temperature over the range from 15 mK to the lowest temperatures attained. These fits confirmed the Curie-Weiss behavior of this LCMN thermometer. Figure 1 compares the LCMN susceptibility to the platinum temperature and demonstrates the stability of the calibration. The data shown are from the final two demagnetizations of the experimental run; the calibration line was determined more than 6 months earlier.

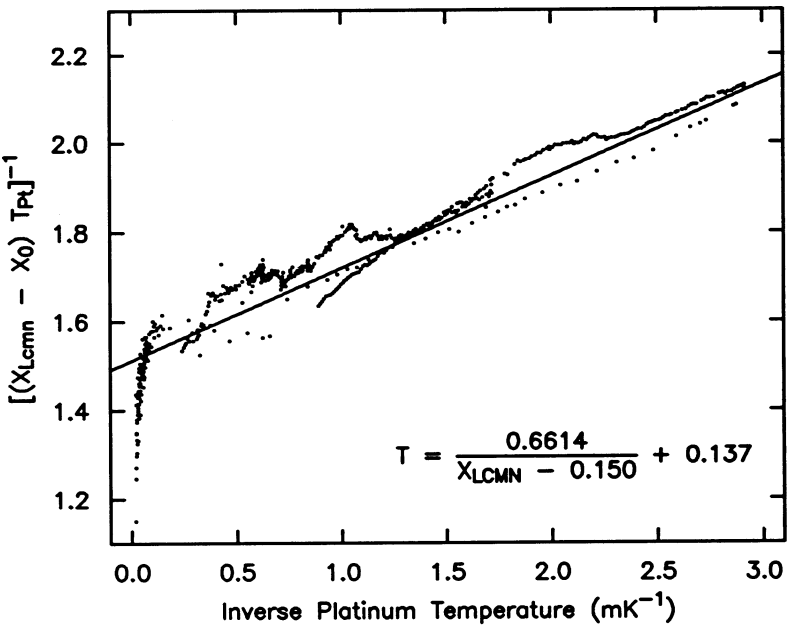

Fig. 1. The Cornell temperature scale, showing the reproducibility of the calibration of the LCMN thermometer. The straight line and the displayed equation are representative of a Curie-Weiss susceptibility. The data points show the relative deviation of the LCMN susceptibility from the platinum temperature for two typical demagnetizations.

2.3. The Texas A&M Temperature Scale

The LCMN susceptibility thermometer used in this experiment was similar to that used at Cornell. This was calibrated[15] at and above 1.1 mK against a ^{3}He melting curve thermometer,[16] with all melting pressure measurements referred to the pressure at the superfluid A transition. The melting curve relation $(P-P_A, T)$ was taken from the data of Halperin *et al.*[17]

The melting curve of ^{3}He provides an excellent thermometry standard for use above the solid ^{3}He ordering temperature $T_s = 1.1$ mK. Resolution and reproducibility of $\sim 10\ \mu$K are available using simple capactive strain gauge sensors and audiofrequency measurement electronics. The $(P-P_A, T)$ relation, as established by Halperin *et al.*,[17] is the only truly thermodynamic temperature scale in use in the millikelvin region. It is based on the Clausius-Clapeyron equation and on the temperature $T_A = 2.752$ mK assigned to the superfluid A transition. The melting curve provides three fixed points, at the A, B, and solid ordering transitions. The chief drawback of melting curve thermometry is that it loses all sensitivity below the solid ^{3}He ordering temperature. The LCMN calibration must therefore be extrapolated from this point downward.

In the calibration procedure followed at Texas A&M, the high-temperature balance point χ_0 of the LCMN bridge was recorded at 1.5 K and was not determined as a low-temperature fitting parameter. The LCMN susceptibility and the temperature, as derived from the melting curve thermometer, were recorded between 45 and 1.1 mK. Using these calibration data and the high-temperature balance point χ_0, it was found that the usual Curie-Weiss formula was inadequate in describing the temperature dependence of the LCMN susceptibility. This was particularly evident when the data were plotted as $[(\chi-\chi_0)T]^{-1}$ vs. $1/T$. This plotting scheme (see Fig. 2) greatly emphasizes the low-temperature behavior of the susceptibility. On such a figure the Curie-Weiss law would appear as a straight line, of intercept $1/C$ and slope Δ/C. To obtain a reasonable fit to the Texas A&M data between 50 and 1 mK, two correction terms must be added to the denominator of the Curie-Weiss formula. A better fit, with the same number of parameters, can be obtained in the form

$$\chi-\chi_0=\frac{1+B_1/T}{A_0T+A_1+A_2/T} \tag{2}$$

The Texas A&M data presented in this paper were analyzed using this fitted function, with parameters

$$\chi_0 = 0.004784, \qquad A_0 = 3.3646 \pm 0.0045$$

$$A_1 = 1.82 \pm 0.62, \qquad A_2 = 0.934 \pm 0.051, \qquad B_1 = 1.00 \pm 0.20$$

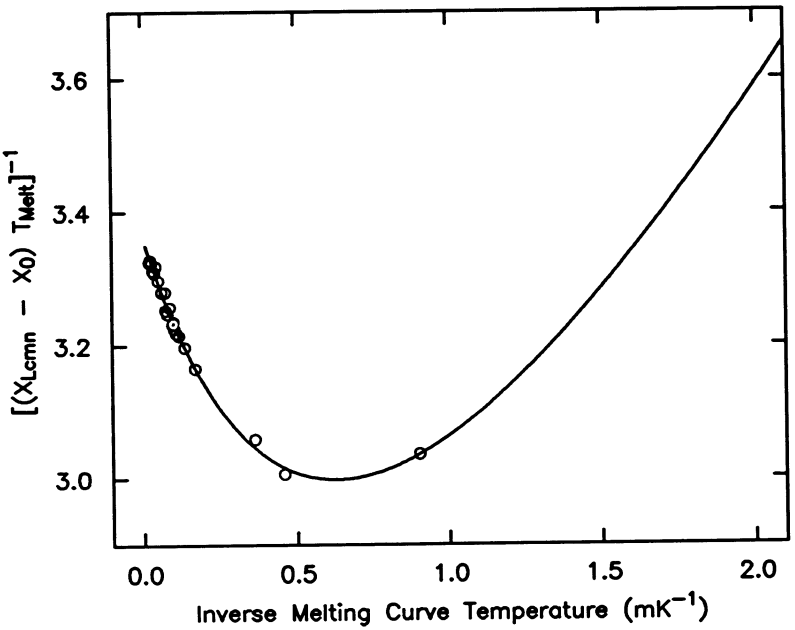

Fig. 2. The Texas A&M temperature scale, showing the calibration of the LCMN susceptibility thermometer from the Halperin (p, T) relation on the ^{3}He melting curve. The fitted line represents a Curie-Weiss susceptibility, with two additional correction terms.

This fit line is plotted with the data in Fig. 2. We defer a comparison of the Cornell and Texas A&M temperature scales to Section 4.

3. TORSIONAL OSCILLATORS AND HYDRODYNAMICS

3.1. The Torsional Oscillators

The oscillators used in these experiments were of a very standard design,[5,7,18,19] illustrated in Fig. 3. Each cell consisted of a thin, disk-shaped cavity for the ^{3}He sample, surrounded by walls of Stycast 1266 epoxy (Emerson and Cuming, Canton, Massachusetts). The interior of the Cornell (Texas A&M) cell was 0.8352 (1.0668) cm in diameter by ~90 (135) μm high. The outer dimensions of the epoxy were 1.27 (1.52) cm diameter by 0.39 (0.79) cm high in the center. The oscillator head was calculated to have, with the electrode vanes included, a moment of inertia of 0.111 (0.405) g cm^2. It was supported on a hollow beryllium-copper torsion rod, 0.051 (0.061) cm i.d., 0.064 (0.068) cm o.d., 0.381 (0.508) cm long, which also served as the fill line for the cell and the thermal link to the demagnetization stage heat exchanger and the thermometers. The torsion constant for

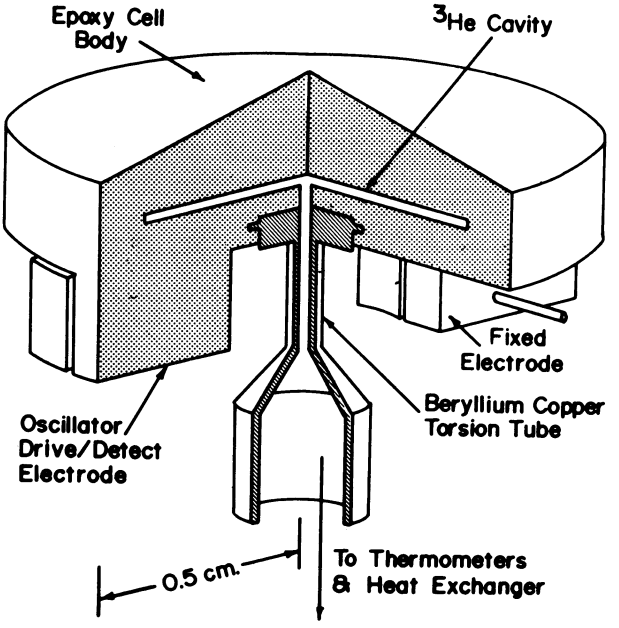

Fig. 3. A torsional oscillator. The cell body and capacitor electrodes are made of Stycast 1266 epoxy. The combination torsion rod and fill line is machined from beryllium-copper. The oscillations are driven and detected capacitively by fixed electrodes mounted on the cryostat and companion plates attached to the oscillator head.

Be-Cu is $\sim 5 \times 10^{11}$ dynes/cm^2; the resonant frequency of the oscillator was $\sim$904 (389) Hz and the low-temperature empty cell Q was $>4 \times 10^5$ (1×10^6).

Motion of the oscillator was driven and detected capacitively using a simple feedback circuit[7] which tracks the resonant frequency and regulates the amplitude. Early measurements at constant drive showed significant nonlinearities, especially at large amplitudes. All data were therefore taken at a constant amplitude of oscillation, with the drive level recorded as a measure of the dissipation in the cell.

3.2. Description of Hydrodynamics

The dissipative and inertial terms governing the behavior of a torsional oscillator are determined by the ratio of the cell height h to the viscous penetration depth $\delta = (2\eta/\rho\omega)^{1/2}$. The viscous penetration depth is a measure of the distance over which the shear waves originating at the walls of the oscillator penetrate into the liquid. Here η is the viscosity, ρ is the

fluid density (replaced by ρ_n in the superfluid), and ω is the angular frequency of oscillation. Figure 4 illustrates the variation of the period and dissipation of an oscillator as the temperature is decreased from $T \approx 40$ mK to the superfluid transition and on through the superfluid phases to the minimum $T \approx 0.5$ mK.

In the normal liquid at high temperatures the viscosity and viscous penetration depth are small. The bulk of the fluid is therefore decoupled from the cell and the dissipation and the period approach their empty-cell values. As the temperature is reduced, the viscosity rises, resulting in an increased penetration depth. This couples more fluid to the walls of the

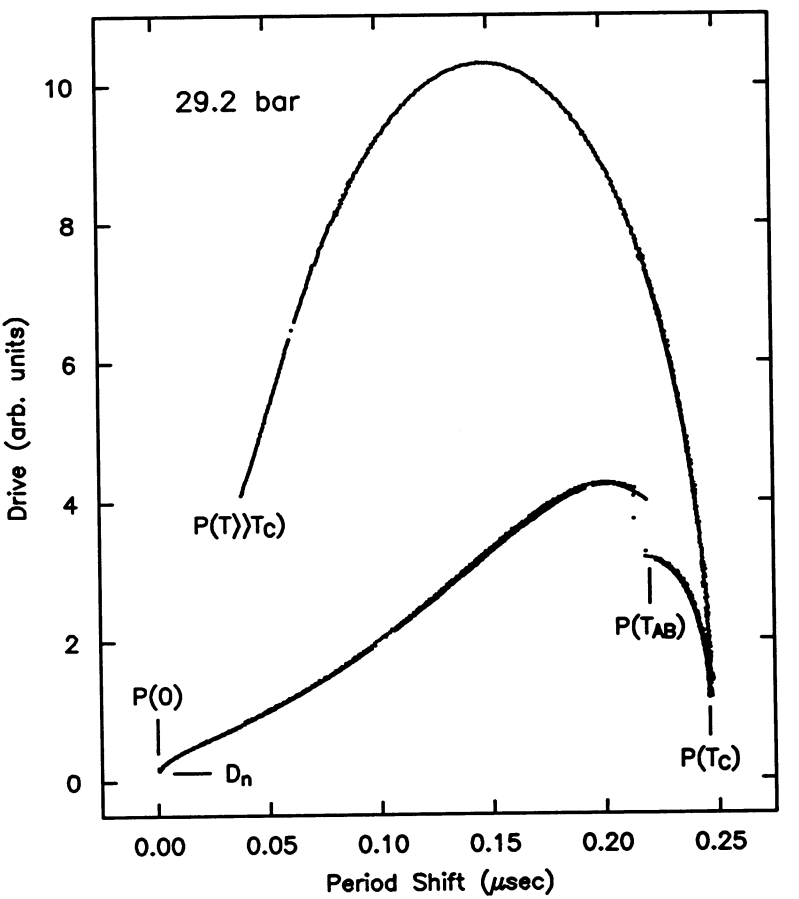

Fig. 4. A sample drive vs. period curve for the torsional oscillator. The dissipation maxima in the normal and superfluid phases and the features at T_c and T_{AB} and as $T \to 0$ are clearly seen.

cell, increasing both the period of oscillation and the dissipation. When the viscous penetration depth approaches half the height of the cell ($h/\delta \approx 2.25$), the drive passes through a maximum. Here the shear waves in the fluid, propagating from the upper and lower cell walls toward the center, begin to overlap substantially. Below this temperature the fluid becomes increasingly well-locked to the cell and the dissipation decreases while the period continues to rise. At the transition temperature the fluid is almost completely locked to the walls of the cell.

Upon entering the superfluid phase, only the normal fraction is coupled to the walls of the oscillator. As the temperature is reduced just below T_c, the viscosity decreases more rapidly than the normal density. The viscous penetration depth therefore drops, the normal fluid unlocks slightly, and the dissipation rises. The monotonic decrease of the period reflects the development of the superfluid fraction, which is stationary and therefore does not contribute to the inertia of the oscillator.

In the A phase, the normal fluid density[5] and viscosity[3] are anisotropic. The values sampled by the oscillator are strongly dependent on the specific textures. These will depend on the cell height, the amplitude of oscillation, and the strength and orientation of any stray magnetic fields. Because of these uncontrolled textural effects, we have not analyzed any A-phase data. We note that a common feature on both cryostats at all pressures above 22 bar is a discontinuity in the period and a large jump in the dissipation at the AB transition.

In the superfluid B phase, the order parameter, and therefore the normal density and viscosity, are isotropic. Textural variations are thus absent and the density results should be independent of the details of the oscillator geometry. A dissipation maximum is seen, but, because of the rapidly changing ρ_n, does not provide a simple relation between the viscous penetration depth and the cell height. As the temperature decreases toward zero the normal density decreases to zero and all of the fluid decouples from the body of the oscillator. In this limit, the drive approaches the "nuisance" drive D_n and the period drops to the empty-cell value $P(0)$.

3.3. Hydrodynamic Equations

In this section we outline the hydrodynamic analysis used to derive the normal fluid density from our measurements of the oscillator period and dissipation. More complete treatments can be found in Ref. 7. An appropriate starting point is the solution to the problem of the motion of a viscous fluid between parallel oscillating plates.[20] This result is applied to the torsional oscillator, taking into account the variation of the surface velocity with radius. Neglecting edge effects and slip, one has that the fluid

exerts a torque on the oscillator

$$T_3 = \pi R^4 \dot{\theta} k \eta \tan(hk/2) \tag{3}$$

where R is the radius of the cell, $\dot{\theta} = i\omega\theta_0 e^{i\omega t}$ is the angular velocity, η is the viscosity, h is the height of the cell, and $k = (1+i)/\delta$, where $\delta = (2\eta/\rho\omega)^{1/2}$ is the viscous penetration depth. Separating the torque into its real and imaginary parts gives

$$T_3 = \beta_1 \dot{\theta} - \beta_2 \ddot{\theta} \tag{4}$$

where

$$\beta_1 = -\omega \frac{\rho_n}{\rho} I_f \frac{1}{x} \frac{\sin x - \sinh x}{\cos x + \cosh x} \tag{5}$$

is the coefficient of the velocity-dependent damping,

$$\beta_2 = \frac{\rho_n}{\rho} I_f \frac{1}{x} \frac{\sin x + \sinh x}{\cos x + \cosh x} \tag{6}$$

is the inertia of the fluid entrained by the motion of the walls,

$$I_f = \tfrac{1}{2}\pi\rho h R^4 \tag{7}$$

is the total fluid moment of inertia, and we have defined $x = h/\delta$, the ratio of the cell height to the viscous penetration depth. The damping and inertia may be related to the measurable parameters $P(T)$, the period, and $Q^{-1}(T)$, the dissipation, by solving the equation of motion for the oscillator. The result for the dissipation is

$$Q^{-1}(T) = \frac{\beta_1}{\omega I_0} = \frac{-\rho_n}{\rho} \frac{I_f}{I_0} \frac{1}{x} \frac{\sin x - \sinh x}{\cos x + \cosh x} \tag{8}$$

and the period of the oscillator is given by

$$\begin{aligned} P(T) &= 2\pi \left(\frac{I_0 + \beta_2}{K} \right)^{1/2} \\ &= 2\pi \left(\frac{I_0}{K} \right)^{1/2} \left(1 + \frac{\rho_n}{\rho} \frac{I_f}{I_0} \frac{1}{x} \frac{\sin x + \sinh x}{\cos x + \cosh x} \right)^{1/2} \end{aligned} \tag{9}$$

where K is the torsion constant for the oscillator. The ratio of I_f to I_0, the ratio of the moment of inertia of the fluid to that of the empty cell, can be simply related to $P(T=0)$, the period with all the fluid decoupled, and $P(T=T_c)$, the period with all the fluid viscously locked to the cell:

$$\frac{I_f}{I_0} = \frac{P(T_c)^2 - P(0)^2}{P(0)^2} \approx \frac{2[P(T_c) - P(0)]}{P(0)} \tag{10}$$

Using Eqs. (8)-(10), we form the function

$$R(x)=\frac{Q^{-1}P(0)^2}{P(T)^2-P(0)^2}=\frac{\sinh x-\sin x}{\sinh x+\sin x} \tag{11}$$

which may be inverted to calculate $x(T)$ from the measured quantities $P(T)$, $Q^{-1}(T)$. Once $x(T)$ is determined, the normal density can be calculated from

$$\frac{\rho_n}{\rho}=\frac{P(T)^2-P(0)^2}{P(T_c)^2-P(0)^2}\,\frac{x(\cos x+\cosh x)}{\sin x+\sinh x} \tag{12}$$

which reduces, in the limits $I_f \ll I_0$ and $x \lesssim 1$, to

$$\frac{\rho_n}{\rho}\approx\frac{P(T)-P(0)}{P(T_c)-P(0)}\left[1+\frac{x^4}{30}+O(x^8)\right] \tag{13}$$

The viscosity may subsequently be determined from the viscous penetration depth and x,

$$\eta=\tfrac{1}{2}\rho_n\omega\delta^2, \qquad \delta=h/x \tag{14}$$

As discussed previously, changes in the oscillator period in the superfluid B phase are chiefly governed by the variation of the normal fraction with temperature. Inverting this relationship, we find that the normal fluid density varies in proportion to the period, with corrections due to the finite unlocking of the fluid from the walls of the cell. These corrections, the terms in x in Eqs. (12) and (13), vary, for $T/T_c \gtrsim 0.5$, from less than 1% at zero pressure to ~5% at 29 bar. At lower temperatures, as the density of normal excitations approaches zero, the fluid unlocks more fully from the cell and the effect of the hydrodynamic correction terms in Eq. (12) can exceed 30%. The temperature dependence of the unlocking parameter x is illustrated in Fig. 5 at several experimental pressures.

An additional complication which can arise in analyzing torsional oscillator results at the lowest temperatures and pressures is that the viscous relaxation time τ_η can approach the characteristic period of the oscillator. In this limit the system would pass out of the hydrodynamic regime and a collisionless transport equation would have to be developed. Fortunately, at the temperatures attained in these experiments, the collisionless limit, $\omega\tau > 1$, was never attained.

3.4. Oscillator Calibrations

The parameters measured during the course of a torsional oscillator experiment are the resonant period and the drive required to run the cell at constant amplitude. The analysis in Section 3.3 is couched in terms of

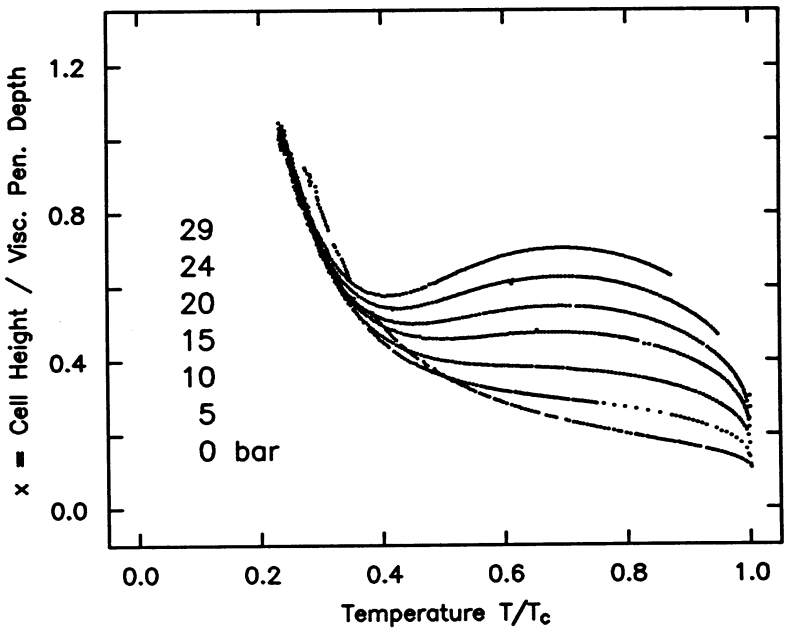

Fig. 5. The viscous unlocking parameter $x = h/\delta$ (the ratio of the cell height to the viscous penetration depth) vs. T/T_c. At low pressures and high temperatures x is small and the normal fluid fraction is nearly equal to the period shift of the oscillator, normalized by the measured $P(0)$ and $P(T_c)$ values.

the period and the ^{3}He fluid dissipation Q^{-1}. The dissipation and drive are simply related, $Q^{-1}_{\text{fluid}} \propto D - D_n$, where D_n is the nuisance drive, related to the intrinsic dissipation in the beryllium-copper torsion rod and the epoxy cell head. To obtain the constant of proportionality, one must, at a single temperature, separately measure the Q of the oscillator and the drive required to maintain the standard amplitude. The Q may be measured in any of several ways. One is to observe the ringdown time of the undriven oscillator. Another is to record the oscillator amplitude as a function of frequency while sweeping through the resonance at constant drive. A third is to use period data and Eq. (11) at the dissipation maximum in the normal fluid, where $x = 2.254$ and $R(x) = 0.7153$. A comparison of these techniques at several pressures gives results identical to within ~2.5%.

In earlier experiments[5,7,18] the pressure-dependent empty-cell period $P(0)$ had to be determined by fitting to the drive as a function of the period in the normal Fermi liquid. To obtain $P(0)$, the fit was extrapolated to its intercept at zero drive and "infinite" temperature. This technique was subject to a systematic error, arising from the observable temperature dependence

of the period of the empty oscillators. In the present experiments we attained temperatures sufficiently low that the normal fluid fraction has decayed nearly to zero. Consequently, the empty-cell period may be determined from a fit to our lowest temperature data. The selection of the correct "empty-cell" parameters is crucial to the determination of the normal density at low temperatures. Small errors in $P(0)$ (and in D_n) will introduce much larger systematic errors in ρ_n/ρ.

At the lowest temperatures the relation between the normal fluid density and the reduced temperature $t = T/T_c$ is particularly simple,

$$\rho_n/\rho \propto t^{-1/2} e^{-\Delta/t} \tag{15}$$

Thus, if we assume that all variations in the period are due to changes in the normal density, we can determine $P(0)$ by fitting to

$$P(T) = P(0) + At^{-1/2} e^{-\Delta/t}, \qquad t \lesssim 0.35 \tag{16}$$

with adjustable parameters $P(0)$, A, and Δ. The quality of this fit, shown in Fig. 6, is comparable to that which determines $P(T_c)$; together they give $P(T_c) - P(0)$ to $\sim 0.05\%$.

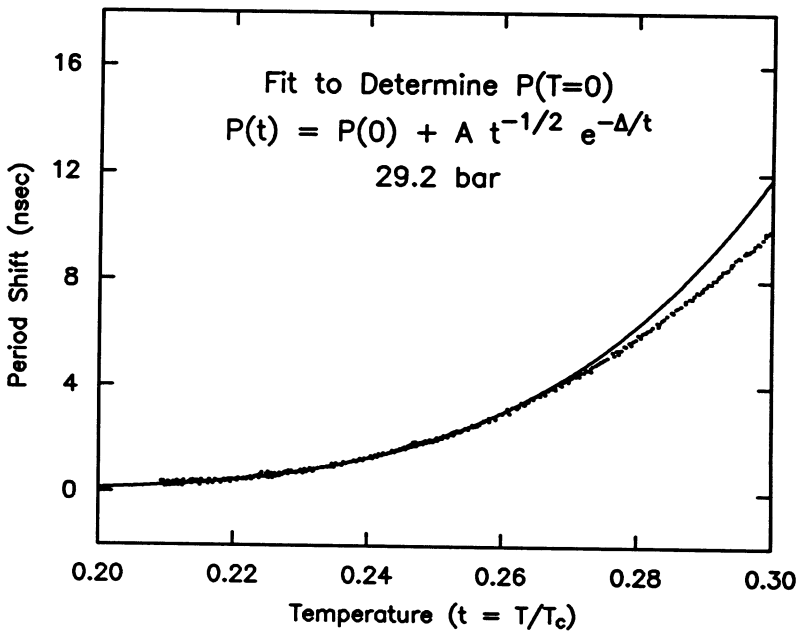

Fig. 6. Result of determining the empty-cell period by fitting to the cell period in the $T \to 0$ limit.

The nuisance drive D_n of the Texas A&M cell was obtained by a direct measurement during the first demagnetization of the experimental series, before any ^{3}He was admitted to the sample volume. The resonant Q of the cell increased as the temperature was reduced, reaching a maximum value $Q_n > 1 \times 10^6$. This Q_n, together with the proportionality constant described previously, determined the nuisance drive used in analyzing all of the Texas A&M data.

The nuisance drive for the Cornell cell was obtained from extrapolations of the drive toward zero temperature at each experimental pressure. These extrapolations were constrained by monitoring their effect on the derived viscous penetration depth and normal density. In the low-temperature limit, the density of normal excitations decays exponentially to zero and all of the fluid decouples from the body of the cell. The residual drive voltage therefore corresponds to the "nuisance" dissipation of the torsion rod and epoxy head. The values found for D_n for the Cornell experiment were relatively pressure independent. Maximum values measured for the Q of the Cornell oscillator were of the order of 4×10^5. The higher Q of the Texas oscillator may in part be due to better vibration isolation than in the Cornell cryostat.

4. RESULTS

4.1. The Normal Fraction

Over the course of the two experiments, a data set consisting of the oscillator period, drive voltage, LCMN susceptibility, and, at Cornell, the platinum susceptibility was acquired at each liquid ^{3}He pressure. The Cornell data were taken while allowing the cryostat to warm relatively slowly and at a uniform rate. A time of approximately 100 h was spent in warming from the minimum temperature to the superfluid transition at each pressure. The warmup rate could be controlled at the higher temperatures by adjusting the power to a resistance wire heater attached to the experimental platform.

At Texas A&M the data acquisition period spanned 4–10 days at each pressure. At night the cryostat was allowed to warm very slowly under its low ambient heat leak. During each day the warmup rate was increased by slowly ramping the magnetic field of the demagnetization solenoid. The day and night warming rates differed by nearly an order of magnitude; no corresponding offsets were observable in the data. The uniform warming rate for the Cornell cryostat was intermediate between the fast and slow rates at Texas A&M. Since the cells and thermometers are of similar design, no significant disequilibrium effects are expected.

The raw period, drive, and LCMN susceptibility data were analyzed to obtain values for the normal density, viscosity, and temperature, according to the procedures outlined in Sections 2 and 3. We have found that the independently determined Cornell and Texas A&M normal density results exhibit a common pressure dependence. In Fig. 7, we plot the derived values of ρ_n/ρ as a function of the reduced temperature $t = T/T_c$.

For constant T/T_c we find that the normal density is an increasing function of pressure. This behavior is due in part to the pressure dependence of the molecular field effects, which enter via the Fermi liquid parameter F_1^s. The magnitude of the superfluid gap parameter Δ may also be subject to temperature- and pressure-dependent corrections due to strong coupling effects. In the weak coupling BCS limit, the temperature dependence of the order parameter enters into the normal density solely through the Yosida function $Y(t)$. Thus,[21]

$$\frac{\rho_n}{\rho} = \frac{(1+\frac{1}{3}F_1^s)\,Y(T)}{1+\frac{1}{3}F_1^s\,Y(T)} \tag{17}$$

We have found that the majority of the pressure dependence shown in Fig. 7 may be attributed to the pressure dependence of the Fermi liquid parameter F_1^s.

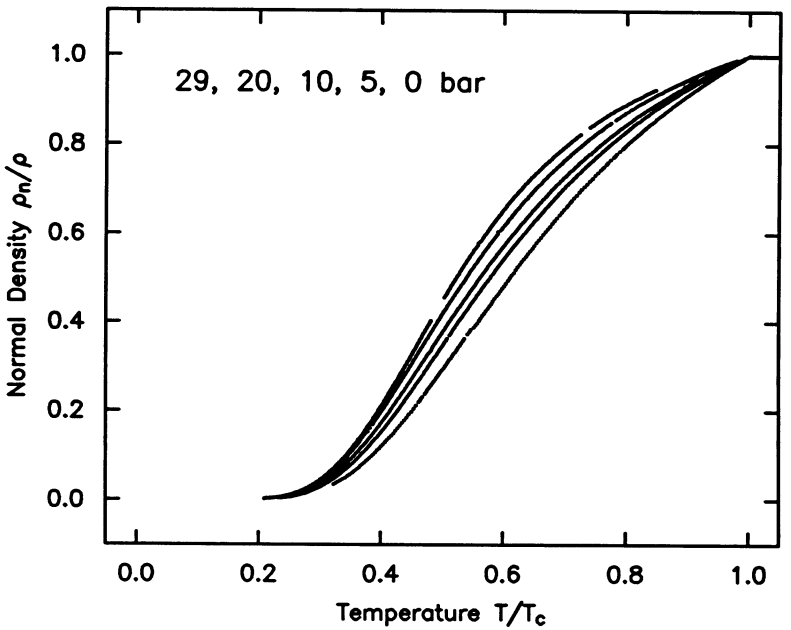

Fig. 7. The temperature and pressure dependence of the normal fluid density. When plotted against T/T_c, results for higher pressures lie above those from lower pressures.

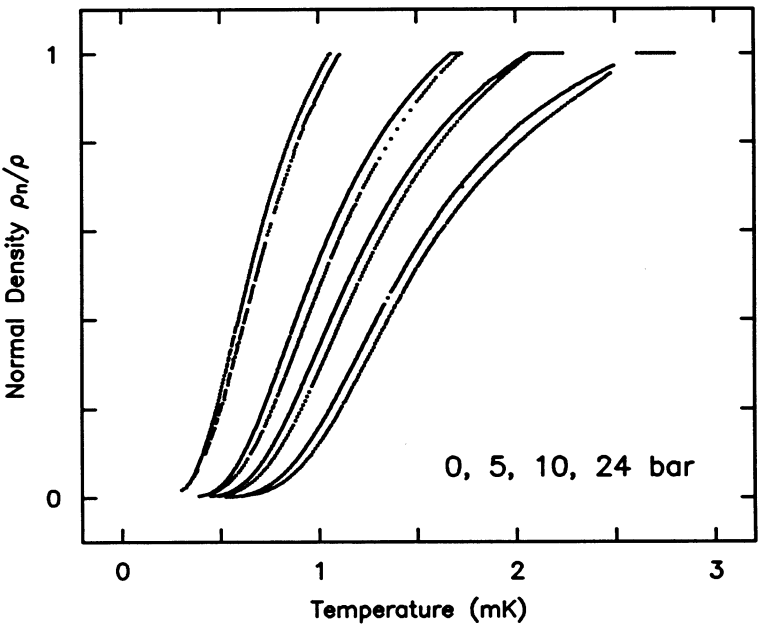

Fig. 8. Normal density results plotted against the Cornell and Texas A&M temperature scales. The Texas A&M data are, at each pressure, to the right of the Cornell data.

At this juncture it is useful to compare the results of our two experiments, before pursuing any further analysis of pressure- and temperature-dependent effects. Figure 8 displays the normal fluid fraction as a function of the absolute temperature at four pressures common to both experiments. It is quite evident that our data do not coincide. The Texas A&M data lie, at each pressure and normal density, at a higher apparent temperature than the Cornell data. This lack of correspondence is not entirely unexpected, since our independent LCMN temperature scales are calibrated from fundamentally different thermometric devices.

4.2. Comparison of Temperature Scales

The simplest comparison between the temperature scales is the traditional comparison of the superfluid transition temperatures T_c at several common pressures. The ratios of the transition temperatures are plotted as open diamonds in Fig. 9. As the ratios vary from less than to greater than unity, neither a simple temperature offset nor a multiplicative factor alone will suffice to bring the scales into agreement. Because a comparison of T_c values is possible over only a limited region in temperature (between $\sim$1

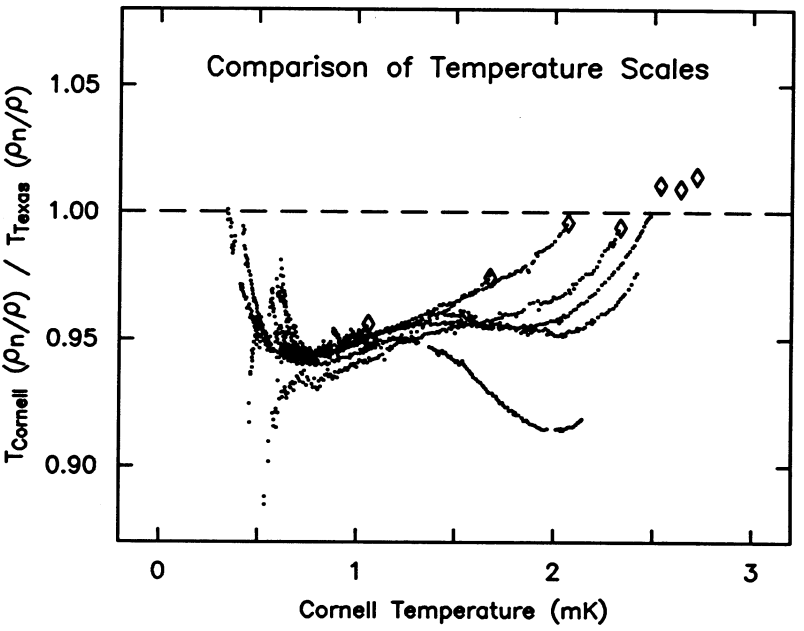

Fig. 9. A comparison of the Cornell and Texas A&M temperature scales, using ρ_n/ρ as a transfer standard. The open diamonds mark the superfluid transition temperatures. All of the data shown were taken in the superfluid B phase.

and ~2.8 mK) and since there are only seven pressures common to both data sets, a direct temperature scale conversion based only on the (T_c, p) points will be of questionable value when extrapolated to our minimum temperatures.

A comparison of the ρ_n/ρ data from our two experiments introduces more rigorous constraints on the temperature scales. This comparison can be extended to temperatures well below 1 mK and will expose any variation of the thermometry with pressure. Therefore, for each common pressure and value of ρ_n/ρ, we have plotted the ratio of the Cornell temperature to the Texas temperature, against the Cornell temperature (see Fig. 9). In principle, these ratios and the ratios of the transition temperatures, plotted earlier, should all fall on a single pressure-independent curve. In fact, there are significant discrepancies at the lowest temperatures and, at the higher pressures, near T_c.

In the low-temperature limit, the diminishing slope of the ρ_n/ρ vs. T/T_c relation will cause small systematic errors in the normal densities to

appear as large offsets in the temperature ratios. These errors can be easily introduced during the determination of the empty-cell periods and the nuisance drives of the oscillators, and are probably responsible for the pressure dependence of the temperature ratios in this region. In addition, the Texas A&M scale, at temperatures below the solid transition on the melting curve, is an extrapolation from a higher temperature calibration. The functional form assumed for this extrapolation will govern the shape of the temperature ratio plot below 1 mK.

In a narrow intermediate region, between ~0.8 and ~1.5 mK, the temperature ratios determined from the comparison of normal density results do fall on a single pressure-independent line. This line is in good agreement with the points defined by the ratios of the transition temperatures, and presumably represents the true difference between the Cornell and Texas A&M temperature scales above 1 mK.

Above 1.5 mK, and for liquid pressures of 15 bar and above, the temperature ratio curves show a significant pressure dependence. This behavior may be indicative of thermal gradients between the torsional oscillators and the thermometers. The thermal time constant defined by the heat capacity of the helium in the cell and the thermal impedance of the narrow torsion tube fill line should increase with temperature and pressure, but should not exceed 200 sec in the vicinity of the A transition at the highest pressures. Comparing the time constants to the warmup rates, one obtains that the temperature error associated with a particular value of ρ_n/ρ should be on the order of a few μK, approximately an order of magnitude smaller than that needed to account for the pressure dependence of the temperature ratios.

Also above 1.5 mK, the main magnet on the Texas A&M cryostat was energized to a field of greater than 1 T, in order to warm up the nuclear stage. This magnetic field may have coupled stray vibrations in the cryostat to parasitic modes of the torsional oscillator, thus altering the dissipation of the pendulum and the apparent normal density. Also, in general, the derivative of the normal density with respect to the absolute temperature decreases as the temperature and pressure increase. The effect of this reduced slope on Fig. 9 will be an exaggeration of the systematic temperature differences in this region relative to comparable differences between 0.8 and 1.5 mK.

We have found no simple explanation for the apparent systematic pressure dependence of the temperature ratios at our lowest and highest temperatures. Barring such an explanation, we cannot correct for the dependence, and therefore have been unable to develop any simple function which might relate our two temperature scales.

4.3. Smoothed Results and Fits

The unresolved systematic differences between our temperature scales are such that any attempts to analyze these normal density results for strong coupling effects and their possible pressure or temperature dependence will be inappropriate. However, since these are presently the most complete sets of ρ_n/ρ measurements available, we have provided three different routes of access to the results.

The smoothed data in Table I are derived from piecewise linear and quadratic fits to the normal density ρ_n/ρ as a function of the reduced temperature $t = T/T_c$. In particular, the Cornell value for ρ_n/ρ at 0 bar and $t = 0.5$ was obtained from a linear fit to the Cornell 0-bar data over the region $0.49 \leq t \leq 0.51$. Values for reduced temperatures $T/T_c < 0.43$ were obtained from quadratic fits, since the curvature of ρ_n/ρ in this region introduces significant errors if linear smoothing is attempted. Quadratic fits for $T/T_c > 0.43$ tended to reproduce the noise in the data, rather than the underlying curvature of the normal density. Linear smoothing was therefore used at these higher temperatures. Gaps in the table correspond to regions in which the data were too sparse to permit reasonable smoothing. This table is the most accurate compact representation of our results.

A less accurate functional representation is achievable via the fit coefficients listed at the bottom of Table I. We have extracted the dominant low-temperature form of the Yosida function,[22,*]

$$Y(t) \sim 3.33 t^{-1/2} e^{-\Delta/t} \tag{18}$$

and fixed the energy gap at $\Delta = 1.1\Delta_{\mathrm{BCS}}(0) = 1.94$. This low-temperature form of the Yosida function is then dressed by the pressure-dependent Fermi liquid corrections, using values for F_1^s from Greywall.[12] A final multiplication by a rational function yields

$$\frac{\rho_n}{\rho} = \frac{(1+\frac{1}{3}F_1^s)(3.33t^{-1/2}e^{-\Delta/t})}{1+\frac{1}{3}F_1^s(3.33t^{-1/2}e^{-\Delta/t})} \frac{1+A_1t+A_2t^2}{1+B_1t+B_2t^2} \tag{19}$$

and introduces enough adjustable parameters (A_1, A_2, B_1, and B_2) to keep the deviation $(\rho_n/\rho)_{\mathrm{data}} - (\rho_n/\rho)_{\mathrm{fit}}$ below ± 0.005 at all temperatures and pressures. An examination of the fitted rational function coefficients in Table I shows no systematic variation with pressure; most of the pressure dependence of the normal density is due to Fermi liquid effects.

*Note that a better approximation, valid to higher T/T_c, is provided in the Appendix to Ref. 9.

TABLE I

Smoothed Values of ρ_n/ρ at Selected Temperatures and all Experimental Pressures[a]

	ρ/ρ_n				
T/T_c	(0.00, 1.059) Cornell	(0.00, 1.108) Texas	(2.18, 1.415) Texas	(4.98, 1.676) Cornell	(5.10, 1.721) Texas
0.22					
0.24				0.0046	
0.26				0.0090	0.0095
0.28		0.0198	0.0192	0.0167	0.0161
0.30		0.0303	0.0288	0.0287	0.0259
0.32		0.0438	0.0415	0.0447	0.0387
0.34	0.0489	0.0589		0.0651	0.0557
0.36	0.0682			0.0898	0.0761
0.38	0.0918	0.1000	0.1008	0.1186	0.1014
0.40	0.1186	0.1249	0.1274	0.1510	0.1296
0.42	0.1480	0.1526		0.1865	0.1615
0.44	0.1809	0.1832	0.1881	0.2242	0.1956
0.46	0.2159	0.2136	0.2224	0.2637	0.2318
0.48	0.2526	0.2483	0.2584	0.3043	0.2703
0.50	0.2906	0.2852	0.2961	0.3453	0.3096
0.52	0.3295	0.3226		0.3860	0.3492
0.54	0.3687	0.3583		0.4262	0.3892
0.56	0.4021	0.3951		0.4655	0.4287
0.58	0.4412	0.4323		0.5037	0.4679
0.60	0.4796	0.4697		0.5406	0.5059
0.62	0.5174	0.5051		0.5761	0.5427
0.64	0.5540	0.5408		0.6102	0.5786
0.66	0.5893	0.5755		0.6428	0.6129
0.68	0.6234	0.6092		0.6738	0.6456
0.70	0.6561	0.6410		0.7037	0.6767
0.72	0.6875	0.6733		0.7320	0.7067
0.74	0.7175	0.7024		0.7586	0.7349
0.76	0.7463	0.7321		0.7839	
0.78	0.7735	0.7603		0.8077	
0.80	0.7994	0.7897		0.8302	
0.82	0.8239	0.8154		0.8516	
0.84	0.8474	0.8437		0.8719	
0.86	0.8700	0.8652		0.8911	
0.88	0.8913	0.8847		0.9093	0.8990
0.90	0.9115	0.9062	0.9133	0.9267	0.9180
0.92	0.9311	0.9267	0.9321	0.9432	0.9368
0.94	0.9498	0.9462	0.9500	0.9587	
0.96	0.9674	0.9646	0.9675	0.9735	0.9696
0.98	0.9844	0.9825	0.9840	0.9870	0.9853
1.00	1.0000	1.0000	1.0000	1.0000	1.0000
F_1^s	5.270	5.270	6.091	7.007	7.044
A_1	−5.546	−1.456	−3.139	−7.047	−5.526
A_2	11.496	3.028	5.984	14.787	11.415
B_1	−4.493	−1.542	−2.744	−5.997	−4.467
B_2	8.466	2.386	4.573	11.574	8.665

Table 1. Continued

	ρ/ρ_n					
T/T_c	(9.96, 2.070) Cornell	(10.00, 2.079) Texas	(15.00, 2.334) Cornell	(15.40, 2.348) Texas	(19.96, 2.508) Texas	(20.5, 2.534) Cornell
0.22	0.0045					0.0036
0.24	0.0066	0.0048	0.0099	0.0046	0.0050	0.0078
0.26	0.0125	0.0090	0.0153	0.0090	0.0094	0.0151
0.28	0.0223	0.0153	0.0254	0.0155	0.0162	0.0265
0.30	0.0361	0.0252	0.0394	0.0257	0.0270	0.0426
0.32	0.0534	0.0389	0.0597	0.0398	0.0418	0.0637
0.34	0.0765	0.0565	0.0855	0.0584	0.0615	0.0894
0.36	0.1041	0.0787	0.1136	0.0818	0.0858	0.1209
0.38	0.1360	0.1044	0.1470	0.1094	0.1148	0.1568
0.40	0.1714	0.1349	0.1841	0.1410	0.1486	0.1960
0.42	0.2094	0.1687	0.2237	0.1765	0.1853	0.2378
0.44	0.2497	0.2503	0.2655	0.2153	0.2253	0.2816
0.46	0.2912	0.2435	0.3079	0.2558	0.2671	0.3268
0.48	0.3331	0.2841	0.3510	0.2968	0.3101	0.3717
0.50	0.3752	0.3249	0.3923	0.3388	0.3535	0.4161
0.52	0.4164	0.3662	0.4334	0.3815	0.3964	0.4594
0.54	0.4570	0.4072	0.4741	0.4231	0.4390	0.5008
0.56	0.4964	0.4478	0.5137	0.4635	0.4799	0.5410
0.58	0.5342	0.4871	0.5514	0.5032	0.5188	0.5794
0.60	0.5705	0.5252	0.5875	0.5410	0.5563	0.6160
0.62	0.6052	0.5621	0.6218	0.5774	0.5918	0.6498
0.64	0.6383	0.5972	0.6542	0.6117	0.6250	0.6819
0.66	0.6695	0.6309	0.6849	0.6442	0.6586	0.7119
0.68	0.6994	0.6628	0.7140	0.6749	0.6861	0.7397
0.70	0.7275	0.6938	0.7410	0.7042	0.7136	0.7657
0.72	0.7539	0.7232	0.7665	0.7315	0.7398	0.7902
0.74	0.7788	0.7496	0.7903	0.7576	0.7648	0.8129
0.76	0.8020	0.7751	0.8127	0.7817	0.7879	0.8341
0.78	0.8243	0.7998	0.8346	0.8050	0.8097	0.8538
0.80	0.8456	0.8226	0.8546	0.8264	0.8306	0.8727
0.82	0.8655	0.8446	0.8733	0.8485	0.8504	0.8897
0.84	0.8840	0.8654	0.8909	0.8691	0.8692	0.9055
0.86	0.9019	0.8852	0.9078	0.8859	0.8872	0.9204
0.88	0.9188	0.9037	0.9235	0.9038	0.9046	0.9344
0.90	0.9355	0.9216	0.9380	0.9206	0.9212	0.9474
0.92	0.9488	0.9384	0.9516	0.9371	0.9373	0.9597
0.94	0.9625	0.9546	0.9646	0.9529	0.9526	0.9712
0.96	0.9762	0.9700	0.9770	0.9675	0.9678	0.9819
0.98	0.9884	0.9850	0.9890	0.9843	0.9835	0.9914
1.00	1.0000	1.0000	1.0000	1.0000	1.0000	1.0000
F_1^s	8.406	8.417	9.710	9.811	10.908	11.028
A_1	−6.125	−6.297	−3.312	−6.931	−7.210	−4.901
A_2	12.558	12.863	7.286	14.774	15.438	8.427
B_1	−5.439	−5.084	−3.230	−5.532	−5.819	−4.552
B_2	10.213	9.979	6.193	11.618	12.363	7.215

[a] For each data set the values in parentheses are, respectively, the pressure p in bar and the temperature T_c in mK. Results from the independent Texas A&M and Cornell measurements are presented as derived, and have not been brought into agreement. Gaps in the table

Table 1. Continued

	ρ/ρ_n					
T/T_c	(24.13, 2.636) Cornell	(24.47, 2.612) Texas	(24.7, 2.654) Cornell	(29.15, 2.680) Texas	(29.2, 2.718) Cornell	
0.22	0.0019		0.0032		0.0032	
0.24	0.0035	0.0051	0.0072	0.0052	0.0076	
0.26	0.0076	0.0095	0.0149	0.0091	0.0153	
0.28	0.0151	0.0165	0.0266	0.0161	0.0275	
0.30	0.0272	0.0273	0.0432	0.0272	0.0445	
0.32	0.0436	0.0427	0.0648	0.0427	0.0668	
0.34	0.0653	0.0628	0.0914	0.0627	0.0946	
0.36	0.0924	0.0880	0.1234	0.0883	0.1279	
0.38	0.1245	0.1183	0.1593	0.1190	0.1663	
0.40	0.1608	0.1529	0.1984	0.1543	0.2085	
0.42	0.2005	0.1907	0.2403	0.1928	0.2541	
0.44	0.2430	0.2319	0.2837	0.2355	0.3012	
0.46	0.2870	0.2750	0.3270	0.2793	0.3495	
0.48	0.3322	0.3183	0.3711	0.3240	0.3980	
0.50	0.3776	0.3629	0.4149	0.3692	0.4462	
0.52	0.4218	0.4062		0.4147	0.4916	
0.54	0.4643	0.4484		0.4563	0.5354	
0.56	0.5048	0.4897		0.4961	0.5767	
0.58	0.5448	0.5283		0.5347	0.6154	
0.60	0.5826	0.5650		0.5705	0.6522	
0.62	0.6171	0.5986		0.6036	0.6858	
0.64	0.6521	0.6300		0.6345	0.7167	
0.66	0.6827	0.6602		0.6631	0.7448	
0.68	0.7106	0.6885		0.6898	0.7708	
0.70	0.7386	0.7150	0.7590	0.7146	0.7948	
0.72	0.7640	0.7399	0.7838	0.7379	0.8173	
0.74	0.7874	0.7630	0.8059	0.7599	0.8380	
0.76	0.8100	0.7851	0.8268	0.7805	0.8574	
0.78	0.8320	0.8064	0.8470	0.8001	0.8750	
0.80	0.8515	0.8265	0.8657	0.8190	0.8906	
0.82	0.8694	0.8455	0.8828	0.8375	0.9053	
0.84	0.8865	0.8636	0.8993	0.8555	0.9193	
0.86	0.9025	0.8814	0.9141	0.8728		
0.88	0.9174	0.8984	0.9284			
0.90	0.9315	0.9149	0.9423			
0.92	0.9447	0.9311	0.9552			
0.94	0.9568	0.9478				
0.96	0.9689					
0.98						
1.00						
F_1^s	11.830	11.910	11.963	13.002	13.002	13.013
A_1	−5.954	−6.750	−7.141	−6.305	−4.520	
A_2	11.581	13.179	16.164	11.070	6.499	
B_1	−5.406	−5.720	−6.282	−5.596	−4.273	
B_2	9.839	10.971	13.511	9.613	5.738	

correspond to regions in which the data were too sparse to permit reasonable smoothing. Parameters obtained by fitting Eq. (19) to each data set are presented below the smoothed results for that data set.

Finally, we have compiled all of our raw period, drive, and LCMN susceptibility data and our derived values for the normal fluid density and temperature onto one magnetic tape. Copies of this tape, at 1600 bpi and in ANSI standard format, may be obtained from the authors.

5. CONCLUSION

In this paper we have described two comprehensive sets of measurements of the temperature and pressure dependence of the normal fluid fraction of superfluid ^{3}He-B. Our results span pressures from 0 to 29 bar and values of ρ_n/ρ from less than 0.005 to unity. The results are presented in tabular and functional form, to allow for their use in the analysis of other hydrodynamic experiments.

The two sets of results are fundamentally inconsistent. The majority of this inconsistency is due to a pressure-independent difference in the temperature scales upon which the measurements are based. Additional, pressure-dependent discrepancies are seen above 1.5 mK, and may be due to complex thermal offsets arising between the thermometers and the torsional pendulums. These differences between the results were exposed by using values of ρ_n/ρ as a transfer parameter for comparing the two temperature scales, and would not have been apparent except through such a comparison.

As a consequence of these differences, primarily thermometric, we have not attempted to extract information about pressure- and temperature-dependent corrections to the BCS weak coupling theory from our normal density results. It is our opinion that, even should there have been no discrepancies in the temperature scales, the present state of thermometry at 3 mK and below is such that the analysis of normal density results for these effects cannot be justified. We suggest that, with the advent of better very low-temperature thermometry, measurements of the normal fluid fraction will play a prominent role in the transfer of temperature scales between laboratories and in increasing our understanding of the strong coupling effects in superfluid ^{3}He.

ACKNOWLEDGMENTS

This research was supported by the National Science Foundation, Division of Materials Research, Low Temperature Physics Program under grants DMR-82-18279 (Texas A&M) and DMR-84-18605 (Cornell), and by the Cornell Materials Science Center through NSF grant DMR-82-17227. J. M. Parpia is the recipient of an A. P. Sloan Research Fellowship. D. G. Wildes was partially supported by an NSF Graduate Fellowship.

We gratefully acknowledge the continuing support of W. P. Kirk, P. Kobiela, and Z. Olejniczak with the thermometry and with the operation of the cryostat over this extended run. The Cornell collaborators acknowledge J. S. Denker and D. F. McQueeney for their development of data acquisition and analysis hardware and software.

REFERENCES

1. H. Kojima, D. N. Paulson, and J. C. Wheatley, *Phys. Rev. Lett.* **32**, 141 (1974).
2. A. W. Yanof and J. D. Reppy, *Phys. Rev. Lett.* **33**, 631, 1030(E) (1974).
3. T. A. Alvesalo, Yu. D. Anufriyev, H. K. Collan, O. V. Lounasmaa, and P. Wennerstrom, *Phys. Rev. Lett.* **30**, 962 (1973); T. A. Alvesalo, H. K. Collan, M. T. Loponen, and M. C. Veuro, *Phys. Rev. Lett.* **32**, 981 (1974); T. A. Alvesalo, H. K. Collan, M. T. Loponen, O. V. Lounasmaa, and M. C. Veuro, *J. Low Temp. Phys.* **19**, 1 (1974).
4. H. Kojima, D. N. Paulson, and J. C. Wheatley, *J. Low Temp. Phys.* **21**, 283 (1975).
5. J. E. Berthold, R. W. Gianetta, E. N. Smith, and J. D. Reppy, *Phys. Rev. Lett.* **37**, 1138 (1976).
6. E. L. Andronikashvilli, *Zh. Eksp. Teor. Fiz.* **16**, 780 (1946).
7. C. N. Archie, T. A. Alvesalo, J. D. Reppy, and R. C. Richardson, *Phys. Rev. Lett.* **43**, 139 (1979); *J. Low Temp. Phys.* **42**, 295 (1981).
8. E. K. Zeise, Ph.D. Thesis, Cornell University, Ithaca, New York (1981), unpublished.
9. D. C. Carless, H. E. Hall, and J. R. Hook, *J. Low Temp. Phys.* **50**, 605 (1983).
10. H. H. Jensen, H. Smith, P. Wolfle, K. Nagai, and T. M. Bisgaard, *J. Low Temp. Phys.* **41**, 473 (1980).
11. R. C. Richardson, in *Proceedings of the 1983 Sanibel Symposium on Quantum Fluids and Solids*, E. D. Adams and G. G. Ihas, eds. (American Institute of Physics, New York, 1983), p. 471.
12. D. S. Greywall, *Phys. Rev. B* **27**, 2747 (1983).
13. J. M. Parpia, W. P. Kirk, P. S. Kobiela, T. L. Rhodes, Z. Olejniczak, and G. N. Parker, *Rev. Sci. Instr.* **56**, 437 (1985).
14. P. M. Berglund, H. K. Collan, G. J. Ehnholm, R. G. Gylling, and O. V. Lounasmaa, *J. Low Temp. Phys.* **6**, 357 (1972); E. Lhota, M. T. Manninen, J. P. Pekola, A. T. Soinne, and R. J. Soulen, Jr., *Phys. Rev. Lett.* **47**, 590 (1981).
15. J. M. Parpia, W. P. Kirk, P. S. Kobiela, and Z. Olejniczak, *J. Low Temp. Phys.* **60**, 57 (1985).
16. D. S. Greywall and P. A. Busch, *J. Low Temp. Phys.* **46**, 451 (1982).
17. W. P. Halperin, F. B. Rasmussen, C. N. Archie, and R. C. Richardson, *J. Low Temp. Phys.* **31**, 617 (1978).
18. J. M. Parpia, D. J. Sandiford, J. E. Berthold, and J. D. Reppy, *Phys. Rev. Lett.* **40**, 565 (1978).
19. J. M. Parpia and T. L. Rhodes, *Phys. Rev. Lett.* **51**, 805 (1983).
20. L. D. Landau and E. M. Lifshitz, *Fluid Mechanics* (Pergamon, London, 1959), p. 93, problem 1.
21. A. J. Leggett, *Rev. Mod. Phys.* **47**, 331 (1975).
22. B. Muhlschlegel, *Z. Phys.* **155**, 313 (1959).